



THE EFFECT OF KINETIC MECHANISM AND TURBULENCE ON THE COMBUSTION PROCESS

E. Affad^{1*}, D. Puechberty², C. Kennel³, M. Assou⁴

¹ Université Hassan II FST de Mohammedia, PB 146, Quartier Yassmina, Morocco

² Université de Rouen place Emile Blondel URA 230 CNRS/CORIA,
76821 Mont Saint Aignan cedex, France

³ Peugeot Citroen (PSA), Route de Gizy, La Garenne Colombes-Paris, France

⁴ Laboratoire de Thermodynamique - Université de Liège, Belgique

* Corresponding author. E-mail: eaffad@hotmail.com

Received : 11 June 2001; revised version accepted 24 January 2002

Abstract

The modelisation of combustion is central problem in most practical combustion system. In this work, turbulent combustion is discussed with a lagrangian model, which is useful for the study of turbulent combustion problem. A coupling between this lagrangian model and the presumed probability density function (pdf) method is used with complex chemistry. The validation of the kinetic mechanism was envisaged before integrated it in the computer code for reciprocating engines. The results of computations with the present models are compared with the experimental results obtained from experience obtained in our laboratory and from PSA (Peugeot – Citroen) engine. The comparisons between the results of the modeling and the experiments showed a good agreement.

Keywords: Combustion; Kinetic mechanism; Reduced mechanism; Detailed mechanism; Emission.

1. Introduction

One of most important theoretical and practical aspects of combustion is the knowledge of the kinetics mechanisms. The use of detailed mechanisms is related to the advent of electronic computers, which permit the solution of large systems of kinetics equations. There is no chance; however, to implement such complex reaction schemes into numerical calculation methods for multidimensional or even turbulent flame. The use of simplified reaction mechanism in describing flame properties for hydrocarbon-air mixture can be traced to the work of Zeldovich and Frank-Kamenetsky (1938) and Semenov (1942). These early formulations were concerned primarily with the prediction of quasi-steady state laminar flame speed. In recent years, however, many combustion problems (that require a time dependent kinetics formulation) have arisen. This kinetics formulation coupled with a fluid mechanics model is used to predict and evaluate overall system performance and properties. Any simplified reaction mechanism that is used must be capable of reproducing experimental flame properties over the range of operating condition under considerations. Many of the simplified kinetics models in common use do not satisfy this requirement and can give erroneous results. In order to choose the good kinetics model we have tested many kinetics mechanisms using a

numerical laminar one-dimensional flame model. This is because if one is especially interested in the chemistry occurring in combustion processes, it is convenient to study this type of flame, since this model of flame is strongly influenced by chemical reaction, and for which the thermodynamics and transport properties for each specie implicate in the mechanisms are very known and that is no effect of turbulence on the combustion. The flame model computations described in this paper have been carried out using the premixed code [1]. The code is used to solve one-dimensional finite difference equations for conservation of mass, momentum, energy and each chemical specie. Transport coefficients, including thermal diffusivity and molecular species diffusivities, have been taken directly from the NASA data [2].

2. The chemistry used

After testing several mechanisms :

- mechanism with 6 reactions that we note (6 reac)
- mechanism with 8 reactions that we note (8 reac)
- mechanism with 9 reactions that we note (9 reac)

we have chosen the following mechanism proposed by Peters et al. [3]:

$C_3H_8 + O + OH$	\rightarrow	$C_2H_4 + CO + H_2O + H_2 + H$
$CO + OH$	\rightarrow	$CO_2 + H$
$H + H$	\rightarrow	H_2
$O_2 + H$	\rightarrow	$OH + O$
$H_2 + OH$	\rightarrow	$H_2O + H$
$H_2 + O$	\rightarrow	$OH + H$
$C_2H_4 + OH$	\rightarrow	$C_2H_2 + H_2O + H$
$C_2H_2 + O_2$	\rightarrow	$2CO + H_2$
$C_3H_6 + O + H$	\rightarrow	$C_2H_4 + CO + H_2O$

Due to space limitations, the expression rates for these reactions may be found in Ref. [3]. This mechanism was derived using steady state assumptions for the intermediate species and partial equilibrium of some elementary reactions. This mechanism implicates 13 participating species and nine global reactions. Steady state approximations have been derived to calculate concentrations of eliminated species from the above non steady state species.

3. Comparison between reduced and detailed mechanisms

3.1 Laminar flame model used

The reduced mechanism is validated further by comparing the predicted species concentration and temperature profiles with those predicted by detailed mechanism in the conditions near of engines and using a numerical laminar one dimensional premixed flame code.

The equations governing steady isobaric, one-dimensional flame propagation are:

- The equation for conservation of mass is :

$$\rho u = \dot{M}. \quad (1)$$

- The continuity equation for species is expressed in the following form :

$$\dot{M} \frac{dY_k}{dx} + \frac{d}{dx} (\rho Y_k V_k A) - A \omega_k W_k = 0. \quad (2)$$

- The conservation of energy is expressed by :

$$\begin{aligned} \dot{M} \frac{dT}{dx} + \frac{1}{c_p} \frac{d}{dx} \left(\lambda A \frac{dT}{dx} \right), \\ - \frac{A}{c_p} \sum_{k=1}^K \rho Y_k V_k c_{pk} \frac{dT}{dx}, \\ + \frac{A}{c_p} \sum_{k=1}^K \omega_k h_k W_k = 0. \end{aligned} \quad (3)$$

these equations are coupled with the following equation of state:

$$\rho = \frac{P \bar{W}}{RT}. \quad (4)$$

In these equations, x denotes the independent spatial coordinate, \dot{M} is the mass flow rate, T is the temperature, Y_k is the mass fraction of the k^{th} specie, P is the pressure, u is the velocity of the mixture, ρ is the mass density, W_k is the molecular weight of the k^{th} specie, \bar{W} is the mean molecular weight of the mixture, λ is the thermal conductivity, c_p is the mean specific heat at constant pressure, ω_k is the molar rate of production of the k^{th} specie per unit volume, h_k is the specific enthalpy of the k^{th} specie and V_k is the diffusion velocity of the k^{th} specie. The flame problem is calculated on the finite interval $0 \leq x \leq 1$.

The boundary conditions are given by:

$$T(0) = T_i, \quad (5)$$

$$Y_k(0) = \varepsilon_k, \quad (6)$$

Where $k=1$ To K (K is the total species number)

$$\left(\frac{dT}{dx} \right)_{x=-\infty, x=+\infty} = 0, \quad (7)$$

$$\frac{dY_k}{dx}(L) = 0, \quad (8)$$

$$\frac{d\dot{M}}{dx} = 0, \quad (9)$$

$$T(x_f) = T_f. \quad (10)$$

x_f is a specified spatial coordinate, T_f is a specified temperature and T_i is the initial temperature of the unburned gas.

3.2 Results of comparison

For space reason, we will present here just the results of computations with the present kinetic

mechanism of propane-air flame at low and high pressure in the case of stoichiometric flames. These results are compared with the computations using the detailed mechanism [3]. In all cases there is reasonable agreement between two predictions as shown in Fig. 1 to Fig. 20. In fact, the agreement was shown for the mole fractions profiles of all species, both stable species and key radical species. The results obtained for the temperature at different values of pressure can be found in Figs 10 and 20. The results are again satisfactory. In fact, there is a little difference relative to flame position that is probably due to thermodynamics and transport properties calculations. As a result, the remaining of this paper we will represent the chemistry by this nine step global reactions due to Peters [3]. This mechanism gives the best results and require a few time calculation compared to these required by 6 reactions and 8 reactions mechanisms used in this work.

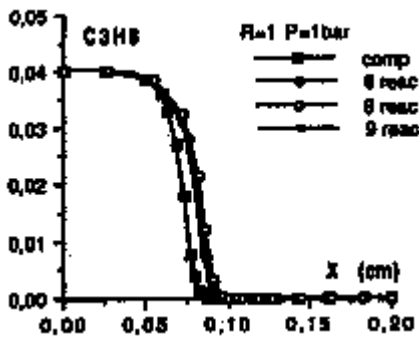


Figure 1 : Mole fraction of fuel.

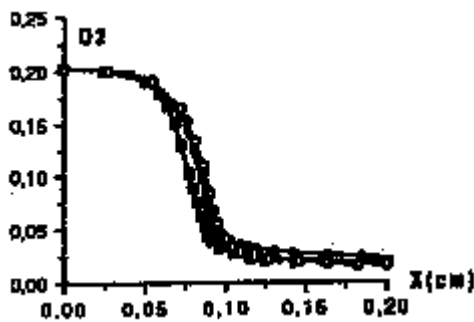


Figure 2 : Mole fraction of oxygen.

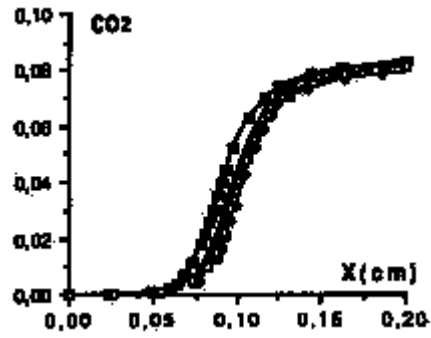


Figure 3 : Mole fraction of fuel CO2.

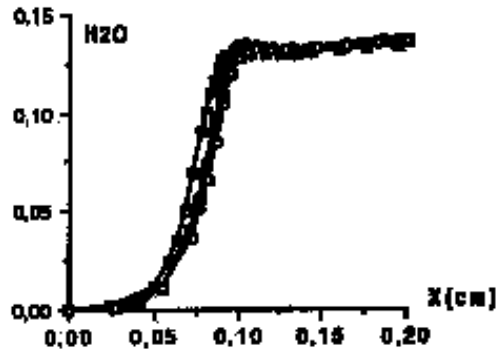


Figure 4 : Mole fraction of H2O.

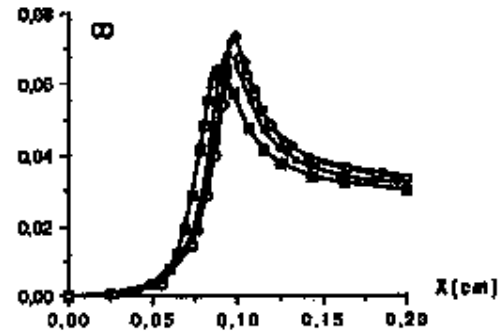


Figure 5 : Mole fraction of CO.

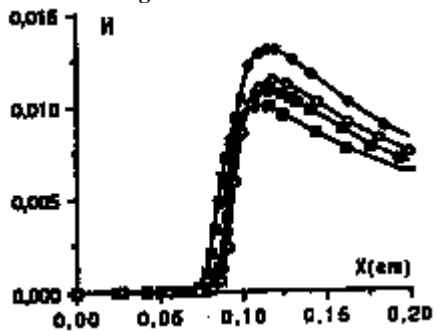


Figure 6 : Mole fraction of H.

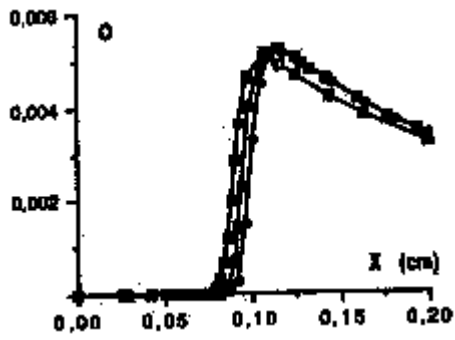


Figure 7 : Mole fraction of O.

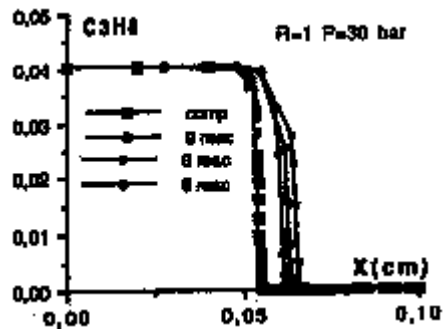


Figure 11 : Mole fraction of fuel.

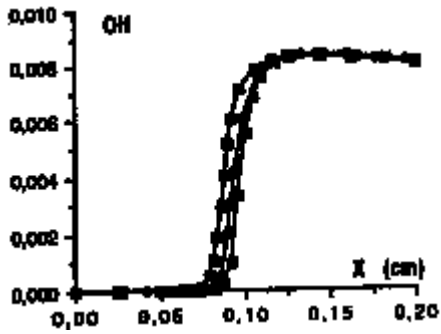


Figure 8 : Mole fraction of OH.

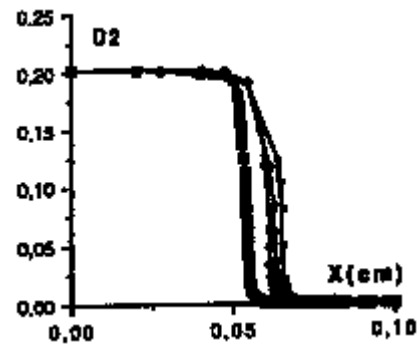


Figure 12 : Mole fraction of O2.

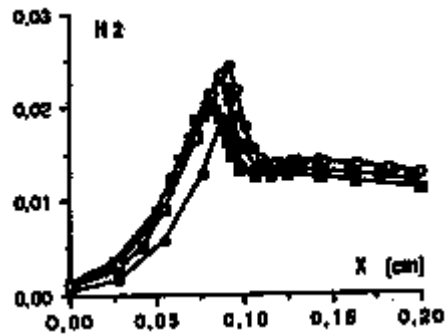


Figure 9 : Mole fraction of H2.

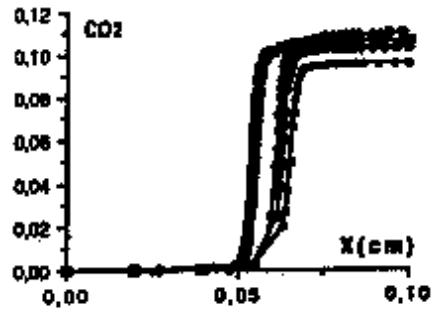


Figure 13 : Mole fraction of CO2.

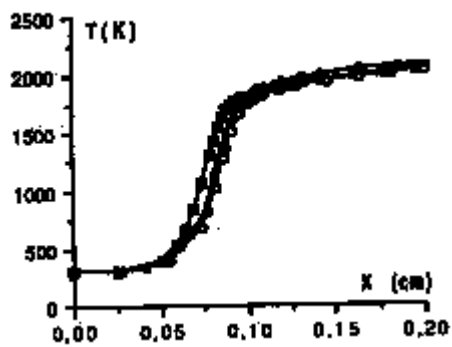


Figure 10 : Temperature profile.

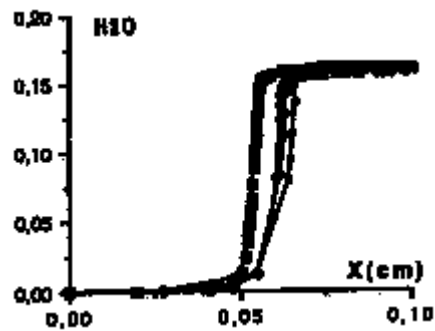


Figure 14 : Mole fraction of H2O

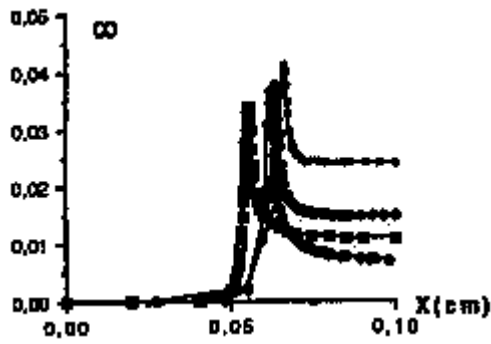


Figure 15 : Mole fraction of CO.

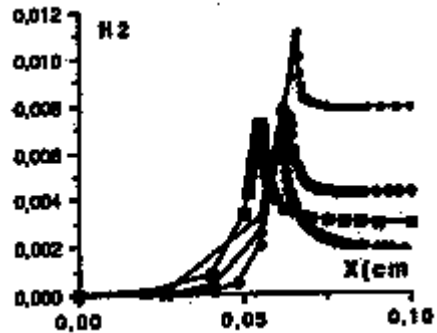


Figure 19 : Mole fraction of H2.

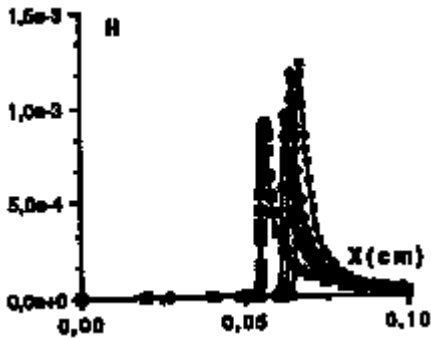


Figure 16 : Mole fraction of H.

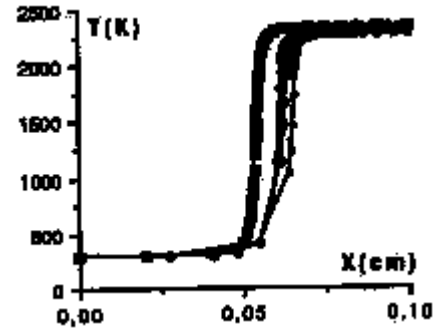


Figure 20 : Profile of temperature.

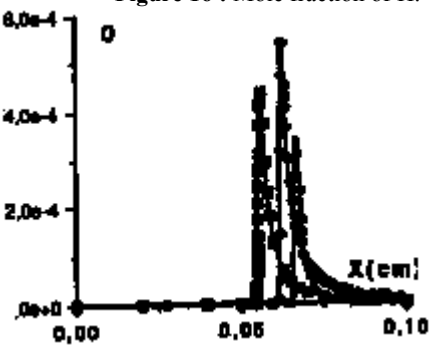


Figure 17 : Mole fraction of O.

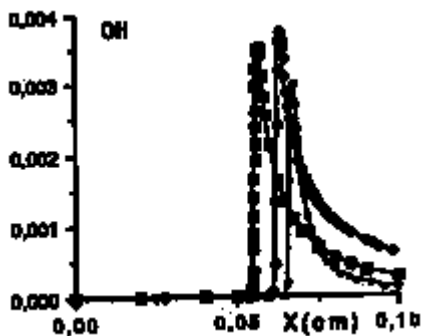


Figure 18 : Mole fraction of OH.

4. Introduction of the chosen mechanism in the numerical code of turbulent combustion

After this validation, we attempted to introduce this scheme in the computer code for reciprocating engines KIVA II [4]. In order to take in to account the effect of turbulence on the combustion process, we have coupled the presumed pdf method to a lagrangian model that we will describe in the following.

4.1 Description of the combustion models

4.1.1 Lagrangian model applied to multireactive mixture

For many years, chemical engineers have been using a lagrangian model called interaction by exchange with the mean (I.E.M), in which the mass fraction of each specie satisfies the lagrangian balance equation:

$$\frac{dY_k}{dT} = \frac{\tilde{Y}_k - Y_k}{\tau_t} + \omega_k, \quad (11)$$

where $k=1$ To K , and

- ω_k is the production rate of the k^{th} specie, and
- K is the species number implicated in the mechanism.

The mass fraction Y_k is randomly fluctuating, due to the turbulent exchange between this fluid particle and the others. The term $\frac{\tilde{Y}_k - Y_k}{\tau_t}$ models these exchange and is the core of the equation which assumes that there is an exchange frequency $\frac{1}{\tau_t}$. The later is known to be depending only on the turbulence itself. Here, we have taken it proportional to $\frac{\varepsilon}{k}$ (k is the turbulent kinetic energy and ε is its dissipation). Assuming for the moment that \tilde{Y}_k are known, the previous equations can be simultaneously integrated to give all Y_k with $k=1$ to K .

4.1.2 The presumed pdf method

The presumed pdf method tries to combine the advantage of pdf method, which is able to take into account the influences of fluctuations on the combustion process. There is another advantage of pdf method that does not require the computation of the full pdf equation, which is enough complicated. This method was proposed for the first time by Mao and Toor [5], and was applied by Lockwood and Nagib [6] in the case of the diffusion flame. If we assume that we can choose a simple shape with peaks and rectangles for pdf as shown in figure 21 depending only on three parameters a, b and c.

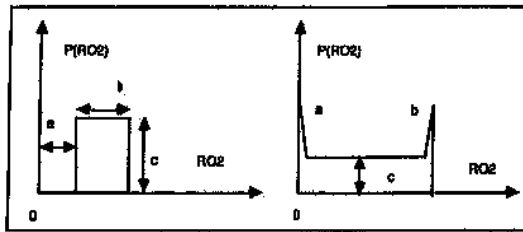


Figure 21 : Presumed shapes of pdf.

These parameters can be computed as a functions of \tilde{Y}_{O_2} and Y'_{O_2} after inverting the following system of equations that one pdf must satisfy :

$$\int_0^1 P(R_{O_2}) dR_{O_2} = 1 \quad (12)$$

and

$$\int P(R_{O_2}) R_{O_2} dR_{O_2} = \tilde{R}_{O_2} \quad (13)$$

where

$$R_{O_2} = \frac{Y_{O_2} - Y_{O_2}^b}{Y_{O_2}^0 - Y_{O_2}^b} \quad (14)$$

with

$$0 \leq R_{O_2} \leq 1 \quad (15)$$

$Y_{O_2}^0$ is the initial mass fraction of oxygen and $Y_{O_2}^b$ is its mass fraction in the burned gas.

ω_k is now implicitly a function of \tilde{Y}_{O_2} and Y'_{O_2} . So, it remains to compute these two terms.

\tilde{Y}_{O_2} is obtained from the euleurian equations, and

Y'_{O_2} require an additional balance equation that can be written as follow :

$$\begin{aligned} & \frac{\delta}{\delta t} (\bar{\rho} Y_{O_2}'^2) + \frac{\delta}{\delta x_\alpha} (\bar{\rho} U_\alpha Y_{O_2}'^2) \\ &= \frac{\delta}{\delta x} (\bar{\rho} U'_\alpha Y_{O_2}'^2) - 2 \bar{\rho} U'_\alpha Y_{O_2}'^2 \frac{\delta Y_{O_2}}{\delta x_\alpha} \\ & - 2 \bar{\rho} d \frac{\delta Y_{O_2}'}{\delta x_\alpha} \frac{\delta Y_{O_2}'}{\delta x_\alpha} + 2 \bar{\rho} d Y_{O_2}'^2 \omega_{O_2} \end{aligned} \quad (16)$$

where d is the diffusion coefficient and $Y_{O_2}' \omega_{O_2}$ can be calculated (in similar way as ω_{O_2} as a

function of \tilde{Y}_{O_2} and Y'_{O_2}) by the following integral :

$$Y_{O_2}' \omega_{O_2} = \int_0^1 P(R_{O_2}) Y_{O_2}' \omega_{O_2}(R_{O_2}) dR_{O_2} \quad (17)$$

we have assumed we can write :

$$U'_\alpha Y_{O_2}' = d \frac{\delta Y_{O_2}'^2}{\delta x_\alpha} \quad (18)$$

and

$$d \frac{\delta Y_{O_2}'}{\delta x_\alpha} \frac{\delta Y_{O_2}'}{\delta x_\alpha} = Z_f \frac{Y_{O_2}'^2}{\tau_t} \quad (19)$$

where Z_f is a constant that we can estimate depending on the configuration geometry. So, if

we know \tilde{Y}_{O_2} and Y'_{O_2} , we know the shape of

pdf and we can calculate the mean production $\tilde{\omega}_k$ for each specie as follow:

$$\tilde{\omega}_k = \int_0^1 P(R_{O_2}) \omega_k(R_{O_2}) d(R_{O_2}) \quad (20)$$

where $\omega_k(R_{O_2})$ is obtained from the integration

of the system (11). So, if we have $\tilde{\omega}_k$ we can integrate the euleurian balance equation for the specie number k and the problem is closed.

4.2 Results of numerical computations

4.2.1 Estimation of the model constant Z_f in the case of the spark ignition engine

The sensitivity of the calculations to the constant Z_f is relatively high, so we must estimate it very precisely. To estimate this constant, the calculations have been performed for an engine with the following characteristics of the calculated chamber:

- equivalence ratio : 0.8,
- volumetric efficiency : 1,
- exhaust gas residual : 0,
- piston with a central bowl,
- rpm : 2500 revolutions/minute,
- connecting rod : 17 cm,
- bore : 10 cm and
- height cylinder : 10.5 cm.

The comparison of a numerical profile of h_{lc} (maximal velocity combustion) versus ca_{50} (crank angle at which 50% of total mass was burned; see figure 32) with the experiment values is shown in figure 22. We can see that the value of Z_f for which the curve $h_{lc}(ca_{50})$ passes near the experimental point (so which gives a good agreement) is $Z_f = 7.75$

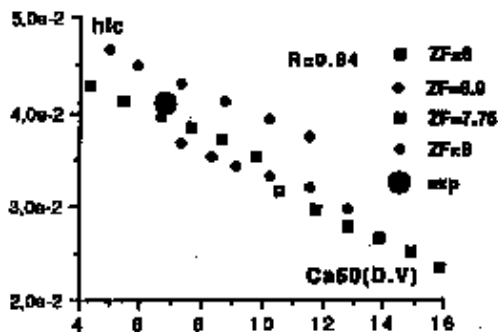


Figure 22 : Evolution of maximal velocity combustion versus Ca50.

4.2.2 Application to estimate the nitrogen oxide (NO) and carbon oxide (CO) emission due to spark ignition engine

The calculations are performed in the same previous conditions. The mechanism used to predict the nitrogen oxide formation is the Zeldovich mechanism. This mechanism coupled with the nine-step mechanism used here allows one to predict the concentration of NO in the combustion chamber.

Figure 23 shows a comparison between predicted NO and the measurements obtained from the PSA (S. A Peugeot Citroen). We can notice that the profile present a maximum for slightly lean flame ($R=0.9$), so the nine step

mechanism used is sensitive to the equivalence ratio of the reaction medium. In figure 24, we can notice that the predicted and the experimental profiles relative to carbon oxide formation at different equivalence ratios show a good agreement for both the lean and the rich flame.

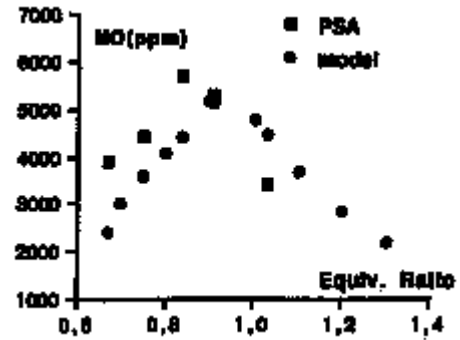


Figure 23 : Profile of nitrogen oxide

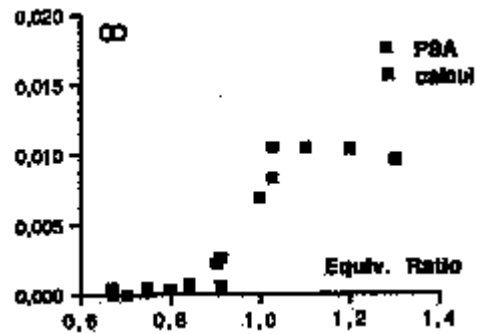


Figure 24 : Mass fraction of carbon oxide.

4.2.3 Comparison with measurements in case of combustion chamber ARC configuration

The combustion device, shown in figure 25 is composed of two main parts: a combustion chamber of 50 x 50 mm square cross section and 100 mm length, and an axisymmetrical, pneumatic driven, single shot piston mounted in a cylinder. Both parts are connected by means of interchangeable performed blocks. Initial turbulence is generated in the combustion chamber by interaction of the jets due to the piston movement towards its top dead center.

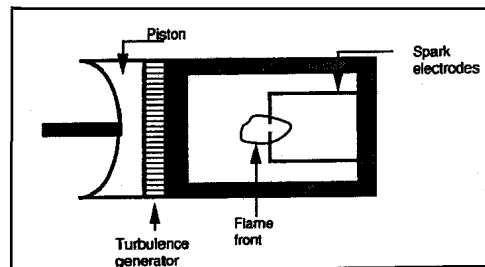


Figure 25 : Schematic of ARC combustion chamber, showing ignition location.

Energy and scales of turbulence can be modified by varying the number and the diameter of the holes in the interchangeable turbulence generator, by adjusting the piston velocity, and by igniting the mixture at different times after the piston arrival. Compression ratio produced is 3. The sparks have duration of 1 ms and store an energy of 3mj.

5. Results

The figs. 26 and 27 show examples of temperature and pressure profiles in the combustion chamber. The constant Z_f is readjusted by comparison between the pressure profile obtained numerically and the experimental one. In this geometry configuration, the value chosen for this constant is now $Z_f = 7.9$. A comparison of the evolution of burnt kernel radius for various equivalent ratio, can be found in figs 28-30. The agreement for the stoichiometric and lean flames is satisfactory. However, the burnt kernel radius is little overpredicted in the case of the rich flame. Fig. 31 shows the effect of turbulence on the flame propagation. The flame kernel begins to grow due to flame propagation and thermal expansion, which is simply the volumetric expansion of the flame kernel as result of heat addition. Another important aspect of flame kernel growth is the effect of turbulence. To first order turbulence convectively distorts or wrinkles the flame kernel, thereby increasing its surface area and proportionately its burning rate. The full effect of turbulence, however, is not immediately felt by the flame kernel, but increases with time until the size and lifetime of the flame kernel exceed multiple of turbulence integral length and time scales respectively. With sufficiently intense turbulence, turbulent strain may cause a reduction in the burning rate even extinction of the flame. Fig. 32 shows a plot of the burned fraction and the velocity combustion as a function of the crank angle.

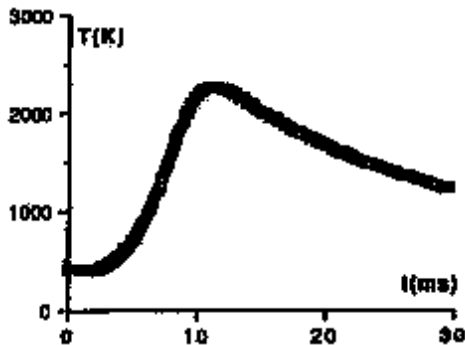


Figure 26 : Temperature profile in ARC combustion chamber.

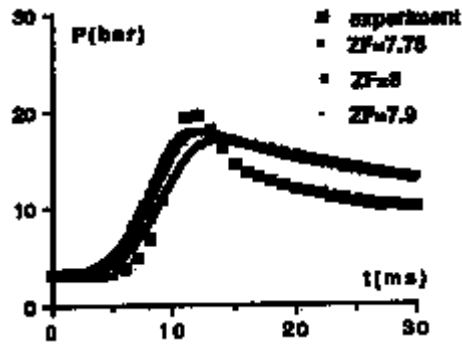


Figure 27 : Pressure profile in ARC combustion Chamber.

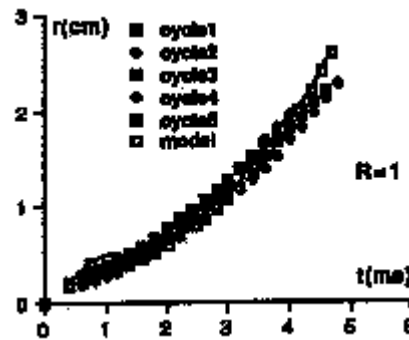


Figure 28 : Evolution of burnt kernel radius.

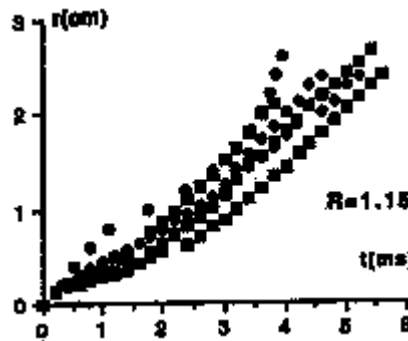


Figure 29 : Evolution of burnt kernel radius.

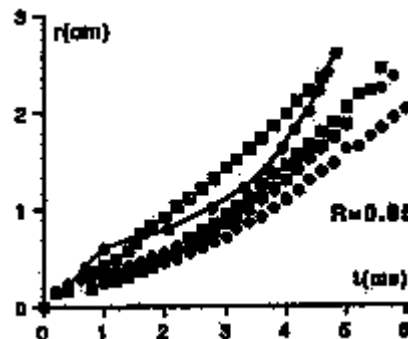


Figure 30 : Evolution of burnt kernel radius.

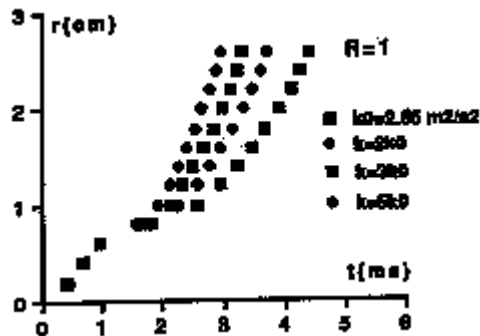


Figure 31 : The effect of turbulence on flame Propagation.

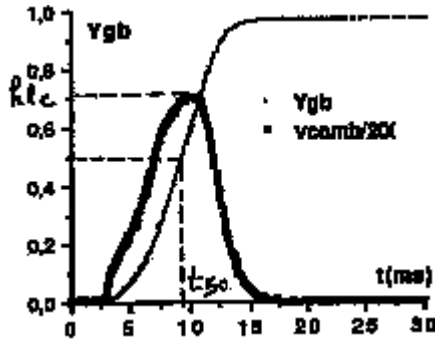


Figure 32 : Evolution of burned fraction (Ygb) and velocity combustion (vcomb).

6. Conclusion

The good scheme is of primary importance for good prediction of turbulent combustion process, so we have attempted to choose a good mechanism. The main findings can be summarized as follow:

- The validation of many mechanisms at different conditions allows us to choose one that gives a good fit and require a few time calculation. This chosen scheme implicates nine-step global reactions, which is due to Peters.
- The use of presumed pdf, Lagrangian model and the integration of this scheme in the computer code for reciprocating engines (Spark Ignition Engines) and combustion chamber ARC gives very encouraging results in the two cases.

References

- [1] R. J. Kee, J. F. Grcar, M. D. Smooke, J. A. Miller, A Fortran program for modeling steady laminar one-dimensional premixed flame Sandia National Laboratories. March 1991.
- [2] M. W. Chase et al. Jannaf thermochemical tables, Third edition, J. Physics. Chem. Ref. Data, 14 Suppl. 1. (1985).
- [3] N. Peters, C. Kennel, F. Mauss, Lecture Notes in Physics, (1992), m15, pp.123-141.
- [4] A. A. Amsden, A computer program for two and three dimensional fluid flows with chemical reactions and fuel sprays, May 31, 1990.
- [5] K. W. Mao, H. L. Toor, AICHE J1, 16 1970; pp. 49-52.
- [6] F. C. Lockwood, A. Naguib, The prediction of the fluctuations in the properties of free round jet, Turbulent diffusion flames, combustion and Flame, 1975; 24 pp. 124-209.
- [7] M. Mouqallid, B. Lecordier, M. Trinité, influence of inhomogeneity of mixing on combustion characteristics in a simulated internal combustion engines, Energy-93, The 5th international Energy Conference, Seoul 1993; vol. 2 pp. 578-592.